https://doi.org/10.5194/tc-2019-183
Preprint. Discussion started: 26 August 2019


The Cryosphere Discussions
Open Access
EGU

# Evaluation of Arctic sea-ice drift and its dependency on near-surface wind and sea-ice concentration and thickness in the coupled regional climate model HIRHAM-NAOSIM

Xiaoyong Yu[1, 2], Annette Rinke[1], Wolfgang Dorn[1], Gunnar Spreen[3], Christof Lüpkes[4], Hiroshi Sumata[4], Vladimir M. Gryanik[4]

[1] Alfred Wegener Institute, Helmholtz Centre for Polar and Marine Research, Potsdam, Germany

[2] School of Marine Sciences, Nanjing University of Information Science and Technology, Nanjing, China

[3] Institute of Environmental Physics, University of Bremen, Bremen, Germany

[4] Alfred Wegener Institute, Helmholtz Centre for Polar and Marine Research, Bremerhaven, Germany

*Correspondence to*: Xiaoyong Yu (xiaoyong.yu@awi.de)

**Abstract.** We examine the simulated Arctic sea-ice drift speed for the period 2003-2014 in the coupled Arctic regional climate model HIRHAM-NAOSIM 2.0. In particular, we evaluate the dependency of the drift speed on the near-surface wind speed and sea-ice conditions. Considering the seasonal cycle of Arctic basin averaged drift speed, the model reproduces the summer-autumn drift speed well, but significantly overestimates the winter-spring drift speed, compared to satellite-derived observations. Also, the model does not capture the observed seasonal phase lag between drift and wind speed, but the simulated drift speed is more in phase with near-surface wind. The model calculates a realistic negative relationship between drift speed and ice thickness and between drift speed and ice concentration during summer-autumn when concentration is relatively low, but the correlation is weaker than observed. A daily grid-scale diagnostic indicates that the model reproduces the observed positive relationship between drift and wind speed. The strongest impact of wind changes on drift speed occurs for high and moderate wind speeds, with a low impact for calm conditions. The correlation under low-wind conditions is overestimated in the simulations, compared to observation/reanalysis. A sensitivity experiment demonstrates the significant effects of sea-ice form drag included by an improved parameterization of the transfer coefficients for momentum and heat over sea ice. However, this does not improve the agreement of the modelled drift speed/wind speed ratio with observations based on reanalysis for wind and remote sensing for sea ice drift. An improvement might be possible, among others, by tuning the open parameters of the parameterization in future.

## 1 Introduction

Arctic sea ice experienced a rapid decrease in recent decades (e.g. Serreze & Stroeve, 2015; Stroeve et al., 2012). On the one hand, the observed Arctic sea-ice decline is caused by thermodynamic processes, such as increasing air and ocean temperatures, e.g. due to ocean heat transports into the Arctic (Serreze et al., 2007). On the other hand, dynamical processes, such as a changed sea-ice drift in response to changing wind, ocean currents and sea-ice conditions (e.g., reduction of sea-ice concentration and thickness), play an important role in the redistribution of sea ice (Rampal et al., 2011; Serreze et al., 2007; Spreen et al., 2011). Except for the fast-ice and shear zones, sea ice moves largely in response to local winds and ocean currents. More than 70% of the variance of the central Arctic pack ice motion is explained by the geostrophic wind alone on the time scale of days to months (Thorndike & Colony, 1982). For compact sea ice in the inner Arctic or sea ice near the coasts, the internal friction can be as large as the forces due to the winds and ocean currents (Leppäranta, 2011). The seasonal Arctic basin-wide sea-ice drift speed, however, is mainly correlated with the sea-ice concentration and thickness, other than with near-surface wind: Sea-ice drift speed decreases with increasing ice concentration when ice concentration is low, and sea-ice drift speed decreases with increasing ice thickness when ice concentration is high (Docquier et al., 2017; Olason & Notz, 2014).

https://doi.org/10.5194/tc-2019-183
Preprint. Discussion started: 26 August 2019




In order to understand and project Arctic sea-ice changes, it is vital for climate models that they can realistically capture the observed sea-ice drift and its dependency on the atmospheric and oceanic forcing and on the sea-ice conditions at different time scales.

Rampal et al. (2011) suggested that the underestimated thinning of Arctic sea ice in the CMIP3 models is related to their failure of capturing the observed acceleration of Arctic sea-ice drift in recent decades. Based on the CMIP5 models and consistent temporal sampling of modeled and observational data, Tandon et al. (2018) showed that only few models capture the observed seasonal cycle of sea-ice drift speed and some models show a seasonal cycle of sea-ice drift in phase with the near-surface wind speed.

Thus, the first aim of this paper is to evaluate the simulated sea-ice drift speed and its relation with sea-ice concentration, thickness and near-surface wind speed in the coupled Arctic regional climate model HIRHAM-NAOSIM 2.0 (Dorn et al., 2019). We use a methodology presented by Olason and Notz (2014) and Docquier et al. (2017) which is appropriate to evaluate the simulated Arctic basin-wide monthly mean drift and its relation to the sea-ice and wind conditions. Since both model evaluations and observational studies based on the daily grid scale are rare, we also present relationship-based diagnostics on daily grid scale.

The second aim of this paper is to explore the sensitivity of the simulated ice drift to the parameterization of the atmospheric near-surface transfer coefficients for heat and momentum over sea ice, in which the effect of sea-ice form drag is included. The air-ice drag controls the sea-ice drift under the influence of the wind forcing. It can be separated into the frictional skin drag due to microscale roughness elements on the sea-ice surface and the form drag caused by large structures like pressure ice ridges and floe edges (Arya, 1973, 1975). Most climate models account for the sea-ice skin drag and consider the form drag only by tuning the spatially and temporally invariant air-ice drag coefficient (Castellani et al., 2018; Tsamados et al., 2014). This approach is poorly constrained by the observations and fails to describe the variability of the air-ice drag processes correctly (Andreas et al., 2010; Lüpkes et al., 2012a; Lüpkes & Gryanik, 2015; Tsamados et al., 2014). Recently, a modern observation-based sea-ice form drag description (Lüpkes & Gryanik, 2015) was implemented into a stand-alone atmospheric model (Renfrew et al., 2019) and a similar parameterization was used by Castellani et al. (2018) as well as by Tsamados et al. (2014) in studies with coupled ice-ocean models. The study of Renfrew et al. (2019) showed an improved agreement of mean atmospheric variables and turbulent fluxes in cold-air outbreak situations over the Fram Strait with measurements when the parameterization including form drag was used. The ice-ocean modelling studies revealed an improvement of the sea-ice drift pattern when form drag was included. We explore within a coupled atmosphere-sea ice-ocean model the impact of the sea-ice form drag caused by ice floe and lead edges on the sea-ice drift. Although the new parameterization contains several parameters which might be tuned for an improvement of model results, we leave optimization of these parameters as future work, and focus on the principal behavior of the model system when form drag is included in the parameterization of atmospheric stress in this study.

This paper is organized in the following way. In Section 2, we describe the model simulations and the observational data as well as the analysis methods used. In Section 3, we present the simulated long-term average Arctic sea-ice drift speed and its dependency on near-surface wind and sea-ice conditions based on both multiyear, Arctic basin-wide scale and daily grid scale. In Section 4, we discuss the sea-ice form drag impact on the atmospheric near-surface turbulent fluxes and on the sea-ice drift speed. Finally, a summary and conclusions are provided in Section 5.

https://doi.org/10.5194/tc-2019-183
Preprint. Discussion started: 26 August 2019


## 2 Data and Analysis

### 2.1 Model and simulations

#### 2.1.1 Coupled atmosphere-ice-ocean regional model

The model used in this study is HIRHAM-NAOSIM 2.0 (Dorn et al., 2019), which consists of the regional atmospheric model HIRHAM5 and the regional ocean-sea ice model NAOSIM (North Atlantic/Arctic Ocean Sea-Ice Model). HIRHAM5 is based on the numerical weather forecast model HIRLAM-7.0 (Undén et al., 2002) and applies the physical parameterizations of the atmospheric general circulation model ECHAM-5.4.00 (Roeckner et al., 2003). Köberle and Gerdes (2003) give a basic description of NAOSIM, while Fieg et al. (2010) describe NAOSIM's fine-resolution model version, which is used in HIRHAM-NAOSIM 2.0. NAOSIM's ocean component is based on the Geophysical Fluid Dynamics Laboratory (GFDL) Modular Ocean Model MOM-2 (Pacanowski, 1996). The sea-ice component is based on the dynamic–thermodynamic sea-ice model described by Harder et al. (1998) and represents an upgrade of the original Hibler (1979) model. The internal ice stress is described by a viscous-plastic rheology according to Hibler (1979). Thermodynamic snow-ice processes are handled using the zero-layer approach by Semtner (1976). Detailed information about HIRHAM-NAOSIM 2.0 is given by Dorn et al. (2019). The model is applied over a circum-Arctic domain at a horizontal resolution of 1/4º (~27 km) in the atmosphere (HIRHAM5) and 1/12º (~9 km) in the ocean (NAOSIM).

#### 2.1.2 Long-term simulations of the base configuration

A 10-member ensemble of multi-decadal climate simulations, covering the 38 years from 1979 to 2016, were carried out with the base configuration of HIRHAM-NAOSIM 2.0, as described by Dorn et al. (2019). These ensemble simulations are referred to as BASE hereafter. The individual ensemble members used the same atmospheric initialization, but applied different ice-ocean initial conditions, which were taken from January 1 of the last 10 years of a preceding 22-year-long coupled spin-up run. The regional model simulations were driven by ERA-Interim reanalysis data (Dee et al., 2011; referred to as ERA-I hereafter). ERA-I provided 6-hourly lateral atmospheric boundary conditions as well as daily surface boundary conditions where required (outside the coupling domain). The lateral ocean boundary conditions in the northern North Atlantic were taken from the Levitus climatology (Levitus and Boyer, 1994; Levitus et al., 1994).

#### 2.1.3 Sensitivity experiments

To investigate the model's sensitivity to the heat and momentum transfer coefficients which explicitly include sea-ice form drag contributions, both a control run (CTRL) and a sensitivity experiment (SENS) for one year (year 2007) were performed. CTRL applies the default atmospheric boundary layer parameterization of ECHAM 5.4 (Roeckner et al., 2003) with air-ice momentum and heat transfer coefficients depending only on atmospheric stability. The sea-ice form drag effect is not included. SENS includes the improved parameterization of air-ice momentum and heat transfer coefficients by Lüpkes and Gryanik (2015). There, the transfer coefficients depend on sea-ice concentration and include both the sea-ice skin drag and form drag effects caused by the edges of ice floes in the marginal sea ice zone and at leads in the inner Arctic. The parameterization could account also for the effect by melt pond edges but this effect would require the knowledge of the pond concentration, which is not available in HIRHAM-NAOSIM. The model applies a flux averaging method, which means that the total flux over a surface covered with sea ice of concentration $A$ and with open water (1-$A$), is the concentration-weighted mean of both contributions. We describe here only the fluxes over sea ice, in which form drag is included in SENS and refer to Roeckner et al. (2003) for the parameterization of fluxes over open water. In the CTRL run (as in the BASE run), however, the air-ice momentum transfer coefficient $C_{d,i}$ and the heat transfer coefficient $C_{h,i}$ include only the sea-ice skin drag effects. They are

https://doi.org/10.5194/tc-2019-183
Preprint. Discussion started: 26 August 2019




calculated as

$$C_{d,i} = C_{dn,i}\, f_{m,i} \quad (1)$$

$$C_{h,i} = C_{hn,i}\, f_{h,i} \quad (2)$$

where $C_{dn,i}$ ($C_{hn,i}$) are the drag (heat transfer) coefficients under neutral atmospheric stratification over ice and $f_{m,i}$ ($f_{h,i}$) are the stability correction functions over ice to adjust $C_{dn,i}$ ($C_{hn,i}$) based on atmosphere stability. $C_{dn,i}$ is calculated as

$$C_{dn,i} = \frac{k^2}{[\ln(z_L/z_{0,i}+1)]^2} \quad (3)$$

where $k$=0.4 represents the v. Karman's constant, $z_L$ is the height of the lowest atmospheric model level, and $z_{0,i}$ represents the skin drag roughness length over sea ice. $C_{hn,i}$ is calculated as

$$C_{hn,i} = \frac{k^2}{\ln(z_L/z_{0,i}+1)\ln(z_L/z_{t,i}+1)} \quad (4)$$

where $z_{t,i}$ represents the scalar roughness length over ice.

In the SENS run, the new momentum transfer coefficient $\hat{C}_{d,i}$ and the new heat transfer coefficient $\hat{C}_{h,i}$ over ice, which both include skin drag and form drag effects, are calculated as

$$\hat{C}_{d,i} = C_{dn,i}\, f_{m,i} + C_{dn,f}\left[f_{m,i}A + f_{m,w}(1-A)\right]/A \quad (5)$$

$$\hat{C}_{h,i} = C_{hn,i}\, f_{m,i} + C_{hn,f}\left[f_{h,i}A + f_{h,w}(1-A)\right]/A \quad (6)$$

where $C_{dn,f}$ ($C_{hn,f}$) represent the form drag (heat transfer) coefficients related to neutral conditions over ice, $f_{m,w}$ ($f_{h,w}$) are the stability correction functions over water to adjust $C_{dn,f}$ as well as $C_{hn,f}$ to atmospheric stability. $C_{dn,f}$ is calculated as

$$C_{dn,f} = C_{e10}\left[\frac{\ln(10/z_{0,f}+1)}{\ln(z_L/z_{0,f}+1)}\right]^2 A(1-A)^{\beta} \quad (7)$$

where $C_{e10}$ represents the effective resistance coefficient (both the aerodynamic resistance coefficient of individual floes and the shape factor), $z_{0,f}$ represents the (form) roughness length, and $\beta$ is a constant exponent describing the dependence of cross wind dimension of a floe on $A$. The values of $C_{e10}$, $z_{0,f}$ and $\beta$ are $2.8\cdot10^{-3}$, $0.57\cdot10^{-3}$ m and 1.1 respectively. $C_{hn,f}$ is calculated as

$$C_{hn,f} = \frac{C_{dn,f}}{1+C_{a,f}\sqrt{C_{dn,f}}} \quad (8)$$

where

$$C_{a,f} = \frac{1}{\mathrm{k}}\ln\left(\frac{z_{0,i}}{z_{t,i}}\right) \quad (9)$$

$$z_{0,i} = 0.69\cdot10^{-3}\ \mathrm{m} \quad (10)$$

$$z_{t,i} = \alpha z_{0,i} \quad (11)$$

$$\alpha = \exp[3.0 - 29.53 z_{0,i}{}^{0.25}] \quad (12)$$

CTRL and SENS simulations comprise each an ensemble of 10 members, which only differ in their ice-ocean initial state. ERA-I provided the boundary forcing as in the BASE simulations.

### 2.2 Datasets for evaluation

#### 2.2.1 Sea-ice drift

For the evaluation of the sea-ice drift speed, satellite-based daily sea-ice drift observations from Kimura et al. (2013) (referred to as KIMURA hereafter) are used. There, the improved maximum cross-correlation method (Kimura & Wakatsuchi, 2000, 2004) were applied to detect ice motions based on AMSR-E brightness temperature. The horizontal resolution of the KIMURA dataset is 60 km x 60 km. Although the accuracy of KIMURA drift speed (1-2 cm $s^{-1}$) is lower than that of buoy data, it has a

https://doi.org/10.5194/tc-2019-183
Preprint. Discussion started: 26 August 2019


much wider spatial and temporal coverage and is therefore appropriate for regional model evaluation (Sumata et al., 2015). Another advantage of the KIMURA product is that it provides ice drift data both in winter and summer. More details are given by Kimura et al. (2013) and Sumata et al. (2015).

In addition, daily sea-ice drift speed from the Pan-Arctic Ice-Ocean Modeling and Assimilation System (PIOMAS; Zhang & Rothrock, 2003) is used. This enables a consistent and simultaneous evaluation of sea-ice drift speed, concentration and thickness, and near-surface wind speed. The PIOMAS data are downloaded from ftp://pscftp.apl.washington.edu/zhang/PIOMAS/data/v2.1/. The mean horizontal resolution in the Arctic is ca. 22 km (Docquier et al., 2017). Detailed information about the PIOMAS dataset is given by Schweiger et al. (2011).

#### 2.2.2 Sea-ice concentration

For sea-ice concentration (SIC), the NSIDC bootstrap daily SIC over Northern Hemisphere Version 3 (https://nsidc.org/data/nsidc-0079) is used. This SIC dataset is based on Nimbus-7 SMMR and DMSP SSM/I-SSMIS passive microwave data. It provides an accuracy of 5-10% and is gridded on the 25 x 25 $km^2$ polar stereographic grid (Comiso, 2017).

#### 2.2.3 Sea-ice thickness

Since Arctic basin-wide long-term sea-ice thickness (SIT) observations are not available, SIT data from PIOMAS are used in this study as a substitute for observational SIT as done in previous studies (Docquier et al., 2017; Johnson et al., 2012; Shu et al., 2015; J. Stroeve et al., 2014). However, we have to recall that PIOMAS is based on a coupled ice-ocean model, even though constrained through the assimilation of observed sea-ice concentrations and sea surface temperatures. Schweiger et al. (2011) showed that the PIOMAS ice thickness agrees with ICESat ice thickness retrievals (in the order of 0.1 m mean difference) and that the spatial thickness patterns agree with each other (pattern correlation coefficients > 0.8). However, PIOMAS appears to overestimate thin ice thickness and to underestimate thick ice (Schweiger et al., 2011).

#### 2.2.4 Near-surface wind

For the near-surface wind speed (WS), daily 10-m wind speed from ERA-I with 0.25º x 0.25º horizontal resolution are used. More information about this dataset is given by Berrisford et al. (2011). The NCEP/NCAR 10- m wind speed with 1.875º x 1.9º horizontal resolution is used to accompany the PIOMAS sea-ice data as this data were used as the wind forcing for PIOMAS. More information about the NCEP/NCAR dataset is given by Kalnay et al. (1996).

### 2.3 Analysis methods

As the different evaluation datasets for sea ice have different spatial resolution, the bilinear interpolation method is used to remap them onto the NAOSIM grid. The common analysis period used in this study is the 12-year-long period 2003-2014 (only December is included for 2012). This limitation is because of the KIMURA data, which are only available since October 2002, and January to November data are missing in 2012 due to transition from AMSR-E to AMSR-2. We focus on summer (JJAS) and winter (DJFM).

The domain for the basin-wide analysis covers the Arctic Ocean (referred to as study domain hereafter; enclosed by the purple line in Figure 1). The study domain is defined following Tandon et al. (2018) and excludes the grid points within a distance of 150 km from each coastline.

The simulations are evaluated by means of the commonly used climatological approach. For this, we present multi-year seasonal mean spatial maps and results spatially averaged over the study domain. The model data represent an average of the 10 ensemble members, which were first averaged spatially over the study domain and then temporally averaged from 2003-

https://doi.org/10.5194/tc-2019-183
Preprint. Discussion started: 26 August 2019




2014. Furthermore, we present evaluation results based on daily data on the grid scale, i.e. for all grid points within the study domain. With this we aim to statistically evaluate the high spatial and temporal variability in the domain, and we represent this by means of box-whisker plots. Therein, the horizontal bar represents the median, the notch represents the 95% confidence interval of the median, the dot represents the mean, the top and bottom of the box represent the 75th and 25th percentiles, and upper/lower whiskers represent the maximum/minimum value within the 1.5 times interquartile range (IQR) to 75/25 percentiles.

Normalized ensemble mean differences between SENS and CTRL run are used to investigate the influence of sea-ice form drag on atmosphere-ice momentum and heat fluxes, sea-ice states and motion and were calculated by dividing ensemble mean differences of SENS minus CTRL with ensemble standard deviations of these differences. Assuming that the differences between two random simulations are normally distributed around zero, the normalized differences enable a rough estimate of the statistical significance of the differences. Normalized differences greater than 2 (3) or lower than -2 (-3) indicate that the difference is significant on the 95 % (99.7 %) level.

## 3 Evaluation of simulated sea-ice drift speed

First, the skill of the BASE simulated mean sea-ice drift speed (SID) is quantified (Section 3.1). SID is forced by the near-surface wind, but it is also influenced by sea-ice roughness and the internal friction. The former is influenced by SIC and the latter is influenced both by SIC and SIT. Therefore, the SID dependency on near-surface wind speed (WS) (section 3.2) and on sea-ice conditions (Sections 3.3-3.4) is evaluated afterwards, in each case in terms of both the climatological and the daily grid-scale views.

### 3.1 Multi-year mean sea-ice drift speed (SID)

The simulated mean SID shows a distinct spatial pattern with highest drift speed near the ice edges in the Barents Sea, Greenland Sea, and Labrador Sea in winter and over the Alaskan coast in summer (Figure 1a). Compared to the KIMURA dataset, the study-domain-mean bias (RMSE) is 1.72 km $d^{-1}$ (2.12 km $d^{-1}$) in winter and -0.03 km $d^{-1}$ (0.91 km $d^{-1}$) in summer. The model generally overestimates SID in the ice edge zone and north of the Canadian archipelago, the region of thickest ice, with a maximum bias of ca. 6 km $d^{-1}$ in winter and a smaller bias in summer (Figure 1b and 1d). This overestimation of SID in the thick-ice region may be linked to the underestimation of SIT and SIC and overestimation of WS over that region (Suppl. Figures S1-S3). The underestimation of SIT and sea-ice volume compared to PIOMAS has been discussed by Dorn et al. (2019) for the longer time period 1979-2016.

The model reproduces the basic mean seasonal cycle of SID compared to the KIMURA data (Figure 2) with respect to timing and absolute values between May and December. The average bias between June and November is almost zero (-0.0003 km $d^{-1}$) and the corresponding RMSE is 0.28 km $d^{-1}$. The maximum ice drift speed (10 km $d^{-1}$) occurs in October both in the model and in the KIMURA data. However, the model substantially overestimates the SID speed in winter and early spring. The averaged bias (RMSE) between December and May reaches 1.52 km $d^{-1}$ (1.64 km $d^{-1}$). In addition, the modeled minimum SID occurs two months delayed in May, compared to the KIMURA data which shows the minimum SID in March. This reflects a longer-lasting and much weaker SID reduction from autumn to the spring season in the model compared to the KIMURA data. Furthermore, the interannual variation of SID is in the model lower than in the KIMURA data (Figure 2). For example, the interannual amplitude is 0.70 km $d^{-1}$ (1.26 km $d^{-1}$) in the model (KIMURA data) in March and 0.36 km $d^{-1}$ (0.74 km $d^{-1}$) in September, respectively.

https://doi.org/10.5194/tc-2019-183
Preprint. Discussion started: 26 August 2019




### 3.2 Dependency of sea-ice drift speed (SID) on near-surface wind speed (WS)

#### 3.2.1 Climatological view

As shown in previous studies (Docquier et al., 2017; Kushner et al., 2018; Olason & Notz, 2014; Tandon et al., 2018), the observed distinct mean seasonal cycle of SID (maximum in autumn, minimum in spring) is obviously not controlled by the wind, which is strongest in winter and weakest in summer (Figure 2). The phase lag between the seasonal cycle of SID and WS is about 3-4 months in observations/reanalysis (KIMURA ice drift/ERA-I wind). The modeled seasonal cycle and magnitude of the WS agrees well with the ERA-I reanalysis. Therefore, according to the delayed SID minimum (section 3.1), the phase lag between the simulated seasonal cycle of SID and WS is reduced to about one month, like in many CMIP3 and CMIP5 models (Rampal et al., 2011; Tandon et al., 2018).

Another metric to quantify the mean relationship between SID and WS is the wind factor, which is the ratio of SID to WS multiplied by 100. Averaged over the study domain, the simulated wind factor is 1.77% in winter and 1.87% in summer, which agrees with the observations/reanalysis (KIMURA ice drift/ERA-I wind) in the sense that the averaged wind factor is larger in summer (1.96%) than in winter (1.42%). However, compared to the observations, the simulated wind factor is too large in winter.

Figure 3 shows the spatial patterns of the multi-year mean wind factor over the Arctic. In winter, the simulated wind factor has its maximum associated with the strong wind and low ice thickness in the Baffin Bay and Greenland Sea. Within the study domain, it has a maximum (~2%) along the Transpolar Drift Stream and minimum values north of Greenland and the Canadian Archipelago (<0.5%) where sea ice is thickest. This pattern is in general agreement with the observation/reanalysis according to KIMURA ice drift/ERA-I wind (Figure 3 and Suppl. Figure S4) and previous results using SSM/I ice drift/NCEP wind (Spreen et al., 2011). However, the simulated wind factor is overestimated compared to the KIMURA/ERA-I data almost everywhere over the study domain in winter, with the maximum bias reaching 1% over the thick ice north of the Canadian Archipelago (Figure 3). In summer, the modelled wind factor peaks (~3%) along the marginal ice zone, such as in the coastal Beaufort Sea. This has been discussed as a result of an enhancement of SID caused by the dynamical coupling between sea ice and coastal ocean (e.g., Nakayama et al., 2012). In contrast to winter, the modelled wind factor is underestimated over the study domain in summer. These seasonally different bias patterns in the wind factor are associated with those of the SID (Figures 1b and 1d).

#### 3.2.2 Daily and grid-scale view

Previous studies reported on the ice drift's nearly linear increase with increasing wind for high and moderate WS (Thorndike & Colony, 1982), but no clear connection for low WS (Leppäranta, 2011; Rossby & Montgomery, 1935). To investigate this in detail, Figures 4 and 5 present the analysis of the dependency of SID on WS based on daily data and on the grid scale. For the observation/reanalysis reference we use KIMURA ice drift and ERA-I wind.

During winter, the simulated SID significantly increases with increasing WS. According to the median values of SID and the associated best fit-line slope of SID vs. WS, the increase of SID varies from 1.31 km $d^{-1}$ to 1.59 km $d^{-1}$ per 1 m $s^{-1}$ WS increase under different SIC classes (Figures 4a and 5a). The strongest SID increase per WS increase occurs for SIC of 50-70% (Figure 4a). In the observations/reanalysis, the SID only consistently increases with increasing WS when SIC is higher than 90% (Figures 4b and 5b). The corresponding slope indicates 0.94 km $d^{-1}$ per 1 m $s^{-1}$, which is a ca. 40% smaller increase than the modeled one. Both the model (for all SIC classes) and the observation/reanalysis (for SIC > 90%) show a linear increase of SID with increasing WS for strong winds (WS > 3 m $s^{-1}$), but a weak dependency of SID on WS for lower winds.

During summer, both the model and the observation/reanalysis agree on a consistent general increase of SID with increasing

https://doi.org/10.5194/tc-2019-183
Preprint. Discussion started: 26 August 2019




WS for all SIC classes when WS > 3 m $s^{-1}$ (Figures 4c, 4d, 5d and 5e). The simulated magnitude of SID increase per 1 m $s^{-1}$ WS increase is similar as in winter. And, again the simulated SID increases faster with increasing WS than in the observation/reanalysis, by about a factor of 2-2.5. Another striking difference between the simulations and observation/reanalysis is that the simulated SID-WS relation shows generally a linear functionality (the relation is slightly weaker when WS ≤ 2 m $s^{-1}$). In contrast, this relation is highly nonlinear in the observation/reanalysis (Figure 4d, 5e); it is only linear for strong winds (WS > 4 m $s^{-1}$). The observed increase of the SID with increasing WS is much stronger when WS passes a threshold (of ca. 4 m $s^{-1}$), compared to lower WS. For weak winds (WS lower than 4 m $s^{-1}$), SID is not much affected by WS changes.

Generally, the observed SID (for a certain WS and SIC class) shows an about 2 times higher spatiotemporal variability (indicated by the larger IQR; Figure 4) than the modelled one. This discrepancy might be linked to a data source difference or inconsistency between the used KIMURA SID observations and ERA-I reanalysis WS data, but it might also hint to a model weakness.

The relation based on PIOMAS (PIOMAS ice drift, NCEP/NCAR wind) is very similar to that in the HIRHAM-NAOSIM 2.0 simulations: SID increases with increasing WS for all SIC classes, both in winter and summer (Figures 5c and 5f). However, the SID-WS relations in PIOMAS are stronger than those in HIRHAM-NAOSIM 2.0 during winter and summer (Figure 5). This may reflect a higher air-ice drag in PIOMAS than in HIRHAM-NAOSIM 2.0.

### 3.3 Dependency of sea-ice drift speed (SID) on sea-ice concentration (SIC)

#### 3.3.1 Climatological view

Previous studies (Docquier et al., 2017; Olason & Notz, 2014) introduced a metric to evaluate the relationship between SID and SIC in terms of the mean seasonal cycle, which we follow here (Figure 6a). An inverse correlation between SID and SIC is expected because a reduction in SIC reduces the internal friction, brings the SID closer to free drift conditions and increases SID. We find such an inverse correlation between SID and SIC both in the model and in observations (KIMURA ice drift, NSIDC bootstrap ice concentration), as well as in PIOMAS from June to September when SIC is low. The corresponding fit line slope in the model is 4.04 km $d^{-1}$ SID increase per 10% SIC decrease, which agree with the slope in observations and in PIOMAS. During the winter months (January to May) when SIC > 95% no such relationship is found neither in observations nor in the models. The SID of the 12 months can be categorized into two groups based on SIC values. Group one for SIC smaller than 95% and group two for SIC larger than 95%. The observed mean SID value in group one (9.23 km $d^{-1}$) is obviously larger than in group two (7.28 km $d^{-1}$). This is also found in PIOMAS. The model reproduces the SID in group one, but largely overestimates the SID in group two. Therefore, the simulated mean SID values in group one (9.24 km $d^{-1}$) and two (8.95 km $d^{-1}$) are quite close to each other. This model deficit may result from the too strong coupling between SID and WS in the model (Figure 2; Section 3.2.1). Following Docquier et al. (2017), we also calculate the slope of SID-SIC best fit line based on data from 12 months, even though there is no clear SID-SIC linear relation over the full year data. The slope based on the model (0.66 km $d^{-1}$ SID increase per 10% SIC decrease) is much weaker than in the observations (6.93 km $d^{-1}$ SID increase per 10% SIC decrease) and in PIOMAS (3.16 km $d^{-1}$ SID increase per 10% SIC decrease). The simulated relation is also much weaker than in the ocean model NEMO-LIM3.6, reported by Docquier et al. (2017). The underestimated relation in the model can be explained by the overestimated SID in winter (Figure 2).

#### 3.3.2 Daily and grid-scale view

On daily grid scale, the model shows an inverse correlation of SID with SIC (Figures 4a, 5a), differently to the climatological view (section 3.3.1). SID increases with decreasing SIC when SIC is larger than ca. 30%. The slopes of the simulated SID-

https://doi.org/10.5194/tc-2019-183
Preprint. Discussion started: 26 August 2019


SIC relation across all the SIC and WS classes vary from 2.89 km $d^{-1}$ to 5.97 km $d^{-1}$ SID increase per 10% SIC decrease. In the observation, the relation is not clear because the median SID uncertainty is very high when SIC is lower than 90% (Figures 4b, 5b). However, the statistically (considering the uncertainty of the median value, represented by the notch) lower SID for high SIC (> 90%) compared to the SID for lower SIC stands out both in observations and simulations. The observations indicate an abrupt drop of SID at 90% SIC. This is in accordance with observations by Shirokov (1977) who showed that SID starts to decrease linearly with increasing SIC, but drops abruptly at a SIC of 90% when internal friction forcing starts its significant influence on SID. This is not reproduced by the simulations.

The model also shows an inverse correlation of SID with SIC for SIC > 20% and WS ≥ 2 m $s^{-1}$ during summer (Figures 4c and 5d). Under different WS classes, the modelled SID-SIC relation varies from 1.40 km $d^{-1}$ to 3.27 km $d^{-1}$ SID increase per 10% SIC decrease. The higher WS is, the stronger is the SID-SIC relation. However, these findings from the simulations are not confirmed by the observations. The observations (KIMURA drift/NSIDC bootstrap ice concentration) do not show an inverse correlation between SID and SIC for all SIC and WS classes in summer (Figures 4d and 5e). Below wind speed of 4 m $s^{-1}$, the observations show a significant relation, but with smaller magnitudes than the model.

The SID-SIC relation in PIOMAS are reversed both in winter and summer when compared to HIRHAM-NAOSIM 2.0: SID increases with increasing SIC when SIC less than 90% (Figures 5c and 5f). This striking feature in PIOMAS suggests that investigations are needed to explain the physically implausible SID-SIC relation in PIOMAS.

Generally, the obvious difference between the SID-SIC relation on multi-year Arctic mean scale and on daily grid scale emphasizes its strong dependency on the temporal and spatial scale.

### 3.4 Dependency of sea-ice drift speed (SID) on sea-ice thickness (SIT)

#### 3.4.1 Climatological view

All datasets (HIRHAM-NAOSIM 2.0 simulations, KIMURA drift/PIOMAS thickness, and PIOMAS drift/PIOMAS thickness) show that SID decreases with increasing SIT (Figure 6b). The SID-SIT fit-line slope calculated based on HIRHAM-NAOSIM 2.0 is 1.10 km $d^{-1}$ SID decrease per 1 m SIT increase. The observed SID-SIT relation is stronger. Data of KIMURA drift/PIOMAS thickness and PIOMAS drift/PIOMAS thickness indicate 2.17 km $d^{-1}$ and 1.83 km $d^{-1}$ SID decrease per 1 m SIT increase, respectively. The weaker simulated dependency of SID on SIT changes is mainly due to the overestimated SID during winter and spring (December to May), when the ice is thick. As pointed out by Olason and Notz (2014), the inverse correlation between drift speed and thickness is physically plausible in winter when concentration is high, but the inverse correlation in summer when concentration is lower, probably only statistical.

#### 3.4.2 Daily and grid-scale view

As in the climatological view, the simulations show generally that SID decreases with increasing SIT (Figures 7a and 7c and Suppl. Figure S5a and 5c), both in winter and summer. In winter, this relation occurs only for SIT smaller than ca. 3.5 m. The simulated SID-SIT relation that calculated based on all thickness categories varies from 0.57 km $d^{-1}$ to 1.08 km $d^{-1}$ SID decrease per 1 m SIT increase across different wind categories(Suppl. Figure S5a). PIOMAS simulates a stronger SID-SIT relation (Suppl. Figure S5c); the slope of the SID-SIT fit-line varies from 0.71 km $d^{-1}$ to 2.77 km $d^{-1}$ SID decrease per 1 m SIT increase, which is larger by a factor of up to 3.5 compared to the simulations.

In summer, the simulated inverse SID-SIT correlation is stronger than in winter, particularly for high WS (Figures 7a and 7c and Suppl. Figures S5a and 5c). The SID-SIT slope varies from 0.49 km $d^{-1}$ to 1.94 km $d^{-1}$ per 1m SIT increase across different wind categories. These values are up to 1.7 times greater than the corresponding values in PIOMAS. This implies that the

https://doi.org/10.5194/tc-2019-183
Preprint. Discussion started: 26 August 2019


modeled relation is generally stronger than in PIOMAS in summer, which is in marked contrast to winter.

Furthermore, Figure 7 confirms the nonlinearity of the SID-WS relation, with a strong impact of WS changes on SID for high and moderate wind speeds, but with a lower impact for low wind speeds (about WS $\leq$ 3 m $s^{-1}$).

**4 Sensitivity to the parameterization including the sea-ice form drag**

In the previous section, we investigated the SID dependency on WS and sea-ice conditions in the BASE simulations, which do not account for the sea-ice form drag. In this section, we analyze how an additional sea-ice form drag influences the near-surface atmospheric fluxes, SID and its dependency on WS and sea-ice condition. For this we compare the one-year ensemble simulations of CTRL (without sea-ice form drag) and SENS (with sea-ice form drag) (see Section 2.1.3 for details). Tsamados et al. (2014) showed that the added form drag mostly improved the sea-ice drift over the summer time. Therefore, our analysis is focused on summer (JJAS).

Figure 8a indicates that the increased ice roughness due to the additional form drag leads to an increased surface momentum flux over most regions of the Arctic Ocean, even though this increase is not significant from a statistical point of view. In few regions the momentum flux does not increase, which indicates that either the neutral drag coefficients over ice is very low or the wind speed and/or atmospheric stratification changed. SID is mainly increased over the marginal ice zone (MIZ) along the Russian coasts (Figure 8b). The spatial pattern of SID change is similar to that of the momentum flux, with pattern correlation of 0.66 (0.76) between their normalized (not normalized) differences. This reveals that the SID increase is mainly associated with an increased momentum flux from the atmosphere to the ice. Related with this, WS decreases over most parts of the Arctic Ocean when sea ice becomes rougher in SENS (Figure 8c). Changes in turbulent heat fluxes, SIC, and 2-m air temperature are small and mixed with regional increases and decreases (Figures 8d-f). Overall, the ensemble mean differences between SENS and CTRL are statistically insignificant, indicating a large across- ensemble scatter due to high internally generated model variability.

Nonetheless, the increase of SID for low SIC in the MIZ and the smaller effect on the more consolidated ice in the central Arctic should imply a stronger Arctic-wide SID-SIC relation. Figures 9 and 10 confirm the stronger increase of SID with decreasing SIC in SENS.

The effect of SIC-dependency, i.e. that the SID change is larger for low SIC, can be explained by the linear dependence of the form drag acting on the floe area on SIC. As lower the SIC as higher the form drag. When SIC is around 90%, the form drag is negligible and thus the drag coefficient in SENS is the same with CTRL.

Furthermore, there is a WS-dependency, i.e. that the SID change is larger for high WS. For example, the SID-SIC relation for calm wind conditions (WS of 1-2 m $s^{-1}$) in SENS is increase of 2.74 km $d^{-1}$ per 10% SIC decrease, which is about 2.4 times stronger than in CTRL. The differences between SENS and CTRL increases even more for high wind speeds. For WS within 9-10 m $s^{-1}$, the SID-SIC relation in SENS is increase of 12.93 km $d^{-1}$ per 10% SIC decrease, which is about 4.8 times stronger than in CTRL. The dependence on wind is complex. Two forces act on the flow, the ocean drag and atmospheric drag. When the ocean drag is much larger than the atmospheric drag (low wind speed), the drift is governed by the ocean drag even if the atmospheric drag doubles. However, when both drags are of comparable size (strong wind) a doubling of the atmospheric drag by increased wind makes a large effect on drift speed. Another impact is due to proportionality of air-ice stress on the square of WS.

https://doi.org/10.5194/tc-2019-183
Preprint. Discussion started: 26 August 2019




## 5 Summary and conclusions

We evaluated the sea-ice drift speed (SID) and its dependency on the near-surface wind and sea-ice conditions (ice concentration and thickness) on multiyear, Arctic-wide mean scale during 2003-2014. Compared with observations, the model does not fully capture the observed SID seasonal cycle, but overestimates SID in winter-spring. Regardless, the model realistically describes the main drivers of the seasonal and long-term variations of Arctic SID: When the sea-ice concentration (SIC) is lower than 95% in summer-autumn, SID increases with decreasing SIC. However, when SIC is higher than 95% in winter, the sea-ice thickness (SIT) is the main factor for SID changes (higher SID for lower SIT). As the simulated SID is overestimated during the cold seasons, the modeled strength of the SID-SIC and SID-SIT relations is underestimated compared with observational data. The SID overestimation during winter in the model cannot simply be attributed to the underestimation of SIT or too strong coupling between SID and WS. Further in-depth analysis of the wintertime sea-ice dynamics and thermodynamics and the atmospheric and oceanic forcing are needed in the future to identify the possible cause of SID overestimation.

The analysis on the daily and grid scale revealed that the SID relations with SIC and SIT are complex due to the large spatiotemporal variation of the sea ice. Based on observations, it is difficult to find a clear relation between SID and SIC. In the model, when SIC is larger than 30%, a higher SIC is accompanied by a significantly lower median SID compared to the SID for lower SIC both in summer and winter. In agreement with the multi-year and Arctic wide findings, the SID decreases with increasing SIT, both in winter and summer. However, in winter, this relation occurs only for high wind speeds. The simulated SID-SIT relation is stronger (weaker) in summer (winter) compared to PIOMAS.

We also evaluated the SID dependency on near-surface wind speed (WS) on the daily and grid scale. The simulated increase of SID with increasing WS is consistent with the observation/reanalysis. Our analysis supports the earlier discussed strong nonlinearity of the SID-WS relation, with a strong impact of WS changes on SID for high and moderate wind speeds, but with only a low impact for lower wind speeds. The weak dependency of SID on WS, when WS is low, was also shown by Lund et al. (2018), based on shipboard marine radar sea-ice drift measurement over the MIZ. This changing relation in the low-wind regime may be caused by the increasing importance of upper-ocean currents for the drift compared to the wind (Lund et al., 2018). Another explanation was given by Leppäranta (2011) and Rossby & Montgomery (1935) who argued that the large-scale wind dominates over the local wind effect.

Finally, we investigated the impact of the changed parameterization of the transfer coefficients for heat and momentum over sea ice on the SID and its dependency on WS and sea-ice conditions. The consideration of sea-ice form drag effects increases the air-to-ice momentum flux and accordingly the SID over most of the Arctic. Largest effects appear for low SIC in the MIZ under high wind conditions. The reason is that in the new parameterization the lower SIC is associated with a potentially larger atmosphere-ice momentum flux, since the form drag contribution is completely transferred to the ice. As a consequence, the increases of SID with decreasing SIC is stronger when the form drag is included.

The implementation of this new parameterization does not improve the simulated SID dependency on WS and sea-ice conditions compared to observations/reanalysis. An improvement might be possible by tuning the open parameters of the parameterization, e.g., similarly as proposed by Renfrew et al. (2019) and Elvidge et al. (2018). A large effect can be expected by a modification of the skin drag coefficient since a large region would be affected and the large observed variability due to pressure ridges allows a test in a wide range of values. Also the inclusion of the melt pond effect on form drag in the model might be beneficial since in the tested version form drag was mainly accounted for only in the marginal sea ice zones but not in the inner ice areas. There, melt ponds cause form drag also during summer (Andreas et al., 2010; Lüpkes et al., 2012a). Adding the form drag from the ocean may further improve the simulated SID-WS relation because the ocean form drag is

https://doi.org/10.5194/tc-2019-183
Preprint. Discussion started: 26 August 2019




normally in the opposite of atmospheric form drag (Lüpkes et al., 2012b). We also cannot exclude systematic biases due to the used reanalysis for the calculation of the wind factor since form drag is not taken into account in the underlying atmospheric model. Therefore, the increased deviation of the simulated SID-WS relation from observations/reanalysis does not necessarily mean the implemented new parameterization worsen the SID-WS relation.

**Data availability.** HIRHAM - NAOSIM model data are available at the tape archive of the German Climate Computing Center (DKRZ; https://www.dkrz.de/up/systems/hpss/hpss); one needs to register at DKRZ to get a user account. We will also make the data available via Swift (https://www.dkrz.de/up/systems/swift) on request. KIMURA sea ice drift data are available at https://ads.nipr.ac.jp/vishop/. The ERA - Interim data were obtained from the European Centre for Medium - Range Weather Forecasts (ECMWF; http://apps.ecmwf.int/datasets/data/interim_full_moda/). The sea - ice concentration data were obtained from the National Snow and Sea Ice Data Center (NSIDC; https://nsidc.org/data/NSIDC - 0051/).

**Author contribution.** X.Y. prepared the manuscript with contributions from all co-authors; Parameterization development: C.L., V.G.; Simulations and Parameterization implementation: W.D.; Assistance with satellite data: H.S., G.S.; Methodology: X.Y., A.R.; Analysis and Visualization: X.Y.; Writing – original draft: X.Y., A.R.; Writing - improving,editing: all co-authors.

**Competing interests.** The authors declare that they have no conflict of interest.

**Acknowledgments.** We gratefully acknowledge the funding by the Deutsche Forschungsgemeinschaft (DFG, German Research Foundation) – Project number 268020496 – TRR 172, within the Transregional Collaborative Research Center "ArctiC Amplification: Climate Relevant Atmospheric and SurfaCe Processes, and Feedback Mechanisms (AC)³". X.Y. was supported by the project "Quantifying Rapid Climate Change in the Arctic: regional feedbacks and large-scale impacts (QUARCCS)" funded by the German and Russian Ministries of Research and Education.

**References**

Andreas, E. L., Horst, T. W., Grachev, A. A., Persson, P. O. G., Fairall, C. W., Guest, P. S., and Jordan, R. E.: Parametrizing turbulent exchange over summer sea ice and the marginal ice zone, Quarterly Journal of the Royal Meteorological Society, 136, 927-943, 2010.

Arya, S. P. S.: Contribution of form drag on pressure ridges to the air stress on Arctic ice, Journal of Geophysical Research (1896-1977), 78, 7092-7099, 1973.

Arya, S. P. S.: A drag partition theory for determining the large-scale roughness parameter and wind stress on the Arctic pack ice, Journal of Geophysical Research (1896-1977), 80, 3447-3454, 1975.

Berrisford, P., Dee, D., Poli, P., Brugge, R., Fielding, K., Fuentes, M., Kallberg, P., Kobayashi, S., Uppala, S., and Simmons, A.: The ERA-Interim archive Version 2.0, ERA Report Series 1, ECMWF, Shinfield Park, Reading, UK, 13177, 2011.

Castellani, G., Losch, M., Ungermann, M., and Gerdes, R.: Sea-ice drag as a function of deformation and ice cover: Effects on simulated sea ice and ocean circulation in the Arctic, Ocean Modelling, 128, 48-66, 2018.

Comiso, J.: Bootstrap sea ice concentrations from Nimbus-7 SMMR and DMSP SSM/I-SSMIS, version 3, NASA National Snow and Ice Data Center Distributed Active Archive Center, Boulder, CO, 2017. 2017.

Dee, D. P., Uppala, S. M., Simmons, A. J., Berrisford, P., Poli, P., Kobayashi, S., Andrae, U., Balmaseda, M. A., Balsamo, G., Bauer, P., Bechtold, P., Beljaars, A. C. M., van de Berg, L., Bidlot, J., Bormann, N., Delsol, C., Dragani, R., Fuentes, M., Geer, A. J., Haimberger, L., Healy, S. B., Hersbach, H., Hólm, E. V., Isaksen, L., Kållberg, P., Köhler, M., Matricardi, M., McNally, A. P., Monge-Sanz, B. M., Morcrette, J. J., Park, B. K., Peubey, C., de Rosnay, P., Tavolato,

https://doi.org/10.5194/tc-2019-183
Preprint. Discussion started: 26 August 2019




C., Thépaut, J. N., and Vitart, F.: The ERA-Interim reanalysis: configuration and performance of the data assimilation system, Quarterly Journal of the Royal Meteorological Society, 137, 553-597, 2011.

Docquier, D., Massonnet, F., Barthélemy, A., Tandon, N. F., Lecomte, O., and Fichefet, T.: Relationships between Arctic sea ice drift and strength modelled by NEMO-LIM3.6, The Cryosphere, 11, 2829-2846, 2017.

Dorn, W., Dethloff, K., and Rinke, A.: Limitations of a coupled regional climate model in the reproduction of the observed Arctic sea-ice retreat, The Cryosphere, 6, 985-998, 2012.

Dorn, W., Rinke, A., Köberle, C., Dethloff, K., and Gerdes, R.: Evaluation of the Sea-Ice Simulation in the Upgraded Version of the Coupled Regional Atmosphere-Ocean- Sea Ice Model HIRHAM–NAOSIM 2.0, Atmosphere, 10, 431, 2019.

Fieg, K., Gerdes, R., Fahrbach, E., Beszczynska-Möller, A., and Schauer, U.: Simulation of oceanic volume transports through Fram Strait 1995–2005, Ocean Dynamics, 60, 491-502, 2010.

Harder, M., Lemke, P., and Hilmer, M.: Simulation of sea ice transport through Fram Strait: Natural variability and sensitivity to forcing, J Geophys Res-Oceans, 103, 5595-5606, 1998.

Hibler, W. D.: A dynamic thermodynamic sea ice model, Journal of physical oceanography, 9, 815-846, 1979.

Johnson, M., Proshutinsky, A., Aksenov, Y., Nguyen, A. T., Lindsay, R., Haas, C., Zhang, J., Diansky, N., Kwok, R., Maslowski, W., Häkkinen, S., Ashik, I., and de Cuevas, B.: Evaluation of Arctic sea ice thickness simulated by Arctic Ocean Model Intercomparison Project models, Journal of Geophysical Research: Oceans, 117, 2012.

Kalnay, E., Kanamitsu, M., Kistler, R., Collins, W., Deaven, D., Gandin, L., Iredell, M., Saha, S., White, G., Woollen, J., Zhu, Y., Chelliah, M., Ebisuzaki, W., Higgins, W., Janowiak, J., Mo, K. C., Ropelewski, C., Wang, J., Leetmaa, A., Reynolds, R., Jenne, R., and Joseph, D.: The NCEP/NCAR 40-Year Reanalysis Project, Bulletin of the American Meteorological Society, 77, 437-472, 1996.

Kimura, N., Nishimura, A., Tanaka, Y., and Yamaguchi, H.: Influence of winter sea-ice motion on summer ice cover in the Arctic, Polar Research, 32, 2013.

Kimura, N. and Wakatsuchi, M.: Increase and decrease of sea ice area in the Sea of Okhotsk: Ice production in coastal polynyas and dynamic thickening in convergence zones, Journal of Geophysical Research: Oceans, 109, 2004.

Kimura, N. and Wakatsuchi, M.: Relationship between sea-ice motion and geostrophic wind in the northern hemisphere, Geophysical Research Letters, 27, 3735-3738, 2000.

Köberle, C. and Gerdes, R.: Mechanisms Determining the Variability of Arctic Sea Ice Conditions and Export, Journal of Climate, 16, 2843-2858, 2003.

Kushner, P. J., Mudryk, L. R., Merryfield, W., Ambadan, J. T., Berg, A., Bichet, A., Brown, R., Derksen, C., Déry, S. J., Dirkson, A., Flato, G., Fletcher, C. G., Fyfe, J. C., Gillett, N., Haas, C., Howell, S., Laliberté, F., McCusker, K., Sigmond, M., Sospedra-Alfonso, R., Tandon, N. F., Thackeray, C., Tremblay, B., and Zwiers, F. W.: Canadian snow and sea ice: assessment of snow, sea ice, and related climate processes in Canada's Earth system model and climate-prediction system, The Cryosphere, 12, 1137-1156, 2018.

Leppäranta, M.: The drift of sea ice, Springer Science & Business Media, 2011.

Lund, B., Graber, H. C., Persson, P. O. G., Smith, M., Doble, M., Thomson, J., and Wadhams, P.: Arctic Sea Ice Drift Measured by Shipboard Marine Radar, Journal of Geophysical Research: Oceans, 123, 4298-4321, 2018.

Lüpkes, C. and Gryanik, V. M.: A stability-dependent parametrization of transfer coefficients for momentum and heat over polar sea ice to be used in climate models, Journal of Geophysical Research: Atmospheres, 120, 552-581, 2015.

Lüpkes, C., Gryanik, V. M., Hartmann, J., and Andreas, E. L.: A parametrization, based on sea ice morphology, of the neutral atmospheric drag coefficients for weather prediction and climate models, Journal of Geophysical Research: Atmospheres, 117, 2012a.

Lüpkes, C., Vihma, T., Birnbaum, G., Dierer, S., Garbrecht, T., Gryanik, V. M., Gryschka, M., Hartmann, J., Heinemann, G., Kaleschke, L., Raasch, S., Savijärvi, H., Schlünzen, K. H., and Wacker, U.: Mesoscale Modelling of the Arctic

https://doi.org/10.5194/tc-2019-183
Preprint. Discussion started: 26 August 2019




Atmospheric Boundary Layer and Its Interaction with Sea Ice. In: Arctic Climate Change: The ACSYS Decade and Beyond, Lemke, P. and Jacobi, H.-W. (Eds.), Springer Netherlands, Dordrecht, 2012b.

Nakayama, Y., Ohshima, K. I., and Fukamachi, Y.: Enhancement of sea ice drift due to the dynamical interaction between sea ice and a coastal ocean, Journal of Physical Oceanography, 42, 179-192, 2012.

Olason, E. and Notz, D.: Drivers of variability in Arctic sea-ice drift speed, Journal of Geophysical Research: Oceans, 119, 5755-5775, 2014.

Pacanowski, R.: MOM 2 documentation user's guide and reference manual. Version 2.0, Geophysical Fluid Dynamics Laboratory Ocean Technical Report. NOAA, GFDL, 232, 1996.

Rampal, P., Weiss, J., Dubois, C., and Campin, J. M.: IPCC climate models do not capture Arctic sea ice drift acceleration: Consequences in terms of projected sea ice thinning and decline, Journal of Geophysical Research, 116, 2011.

Renfrew, I. A., Elvidge, A. D., and Edwards, J. M.: Atmospheric sensitivity to marginal-ice-zone drag: local and global responses, Quarterly Journal of the Royal Meteorological Society, doi: 10.1002/qj.3486, 2019. 2019.

Roeckner, E., Bäuml, G., Bonaventura, L., Brokopf, R., Esch, M., Giorgetta, M., Hagemann, S., Kirchner, I., Kornblueh, L., and Manzini, E.: The atmospheric general circulation model ECHAM 5. PART I: Model description, 2003. 2003.

Rossby, C.-G. and Montgomery, R. B.: The layer of frictional influence in wind and ocean currents, Massachusetts Institute of Technology and Woods Hole Oceanographic Institution, 1935.

Schweiger, A., Lindsay, R., Zhang, J., Steele, M., Stern, H., and Kwok, R.: Uncertainty in modeled Arctic sea ice volume, Journal of Geophysical Research, 116, 2011.

Semtner, A. J.: A model for the thermodynamic growth of sea ice in numerical investigations of climate, Journal of Physical Oceanography, 6, 379-389, 1976.

Serreze, M. C., Holland, M. M., and Stroeve, J.: Perspectives on the Arctic's Shrinking Sea-Ice Cover, Science, 315, 1533-1536, 2007.

Serreze, M. C. and Stroeve, J.: Arctic sea ice trends, variability and implications for seasonal ice forecasting, Philosophical Transactions of the Royal Society A: Mathematical, Physical and Engineering Sciences, 373, 20140159, 2015.

Shirokov, K.: Vliyanie splochennosti na vetrovoj dreif l'dov, Sb. Rab. Leningr. GMO, 9, 46-53, 1977.

Shu, Q., Song, Z., and Qiao, F.: Assessment of sea ice simulations in the CMIP5 models, The Cryosphere, 9, 399-409, 2015.

Spreen, G., Kwok, R., and Menemenlis, D.: Trends in Arctic sea ice drift and role of wind forcing: 1992–2009, Geophysical Research Letters, 38, 2011.

Stevens, D. P.: The Open Boundary Condition in the United Kingdom Fine-Resolution Antarctic Model, Journal of Physical Oceanography, 21, 1494-1499, 1991.

Stroeve, J., Barrett, A., Serreze, M., and Schweiger, A.: Using records from submarine, aircraft and satellites to evaluate climate model simulations of Arctic sea ice thickness, The Cryosphere, 8, 1839-1854, 2014.

Stroeve, J. C., Serreze, M. C., Holland, M. M., Kay, J. E., Malanik, J., and Barrett, A. P.: The Arctic's rapidly shrinking sea ice cover: a research synthesis, Climatic Change, 110, 1005-1027, 2012.

Sumata, H., Kwok, R., Gerdes, R., Kauker, F., and Karcher, M.: Uncertainty of Arctic summer ice drift assessed by high-resolution SAR data, Journal of Geophysical Research: Oceans, 120, 5285-5301, 2015.

Tandon, N. F., Kushner, P. J., Docquier, D., Wettstein, J. J., and Li, C.: Reassessing Sea Ice Drift and Its Relationship to Long-Term Arctic Sea Ice Loss in Coupled Climate Models, Journal of Geophysical Research: Oceans, 123, 4338-4359, 2018.

Thorndike, A. S. and Colony, R.: Sea ice motion in response to geostrophic winds, Journal of Geophysical Research: Oceans, 87, 5845-5852, 1982.

Tsamados, M., Feltham, D. L., Schroeder, D., Flocco, D., Farrell, S. L., Kurtz, N., Laxon, S. W., and Bacon, S.: Impact of variable atmospheric and oceanic form drag on simulations of Arctic sea ice, Journal of Physical Oceanography, 44,

https://doi.org/10.5194/tc-2019-183
Preprint. Discussion started: 26 August 2019




575 1329-1353, 2014.

https://doi.org/10.5194/tc-2019-183
Preprint. Discussion started: 26 August 2019




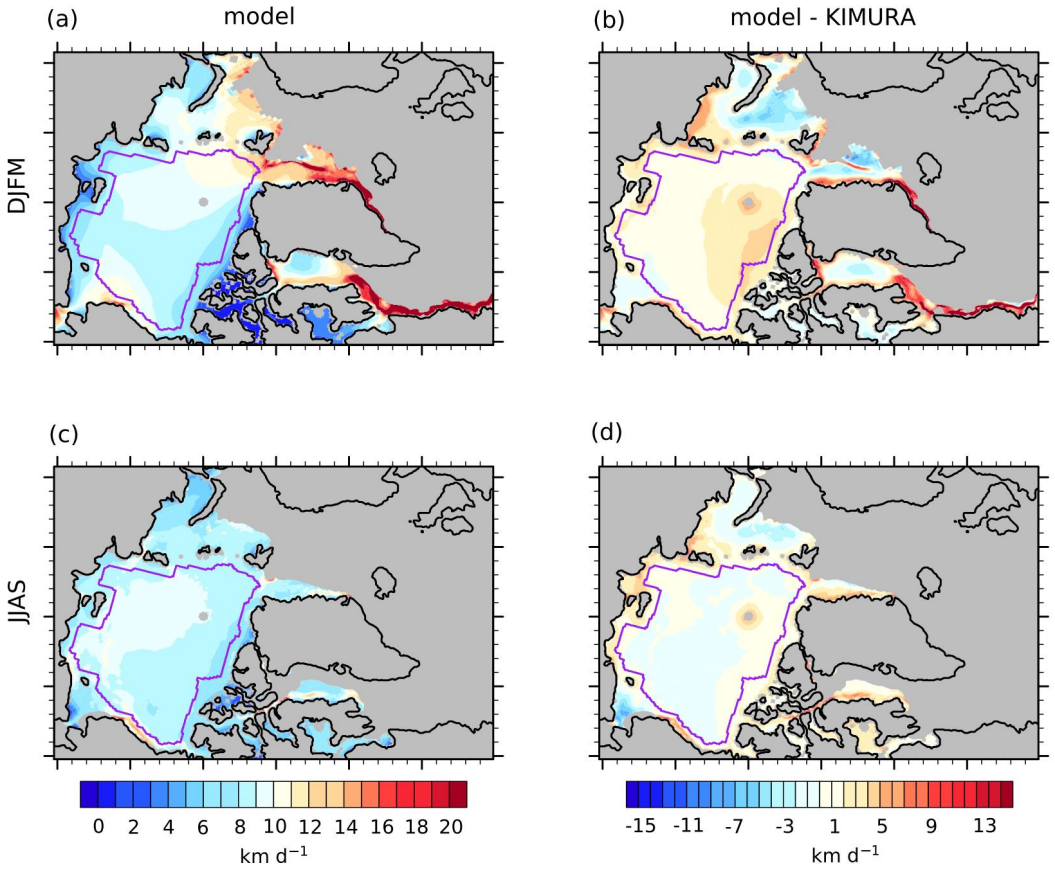


**Figure 1**: Mean spatial pattern of sea-ice drift speed [km d$^{-1}$] in the model (ensemble mean) during 2003-2014 (a) winter (DJFM) and (c) summer (JJAS). (b) and (d) are the model differences to the observation ("Model - KIMURA") during winter and summer respectively. The purple line in each panel indicates the study domain used for the basin-wide analysis.

https://doi.org/10.5194/tc-2019-183
Preprint. Discussion started: 26 August 2019




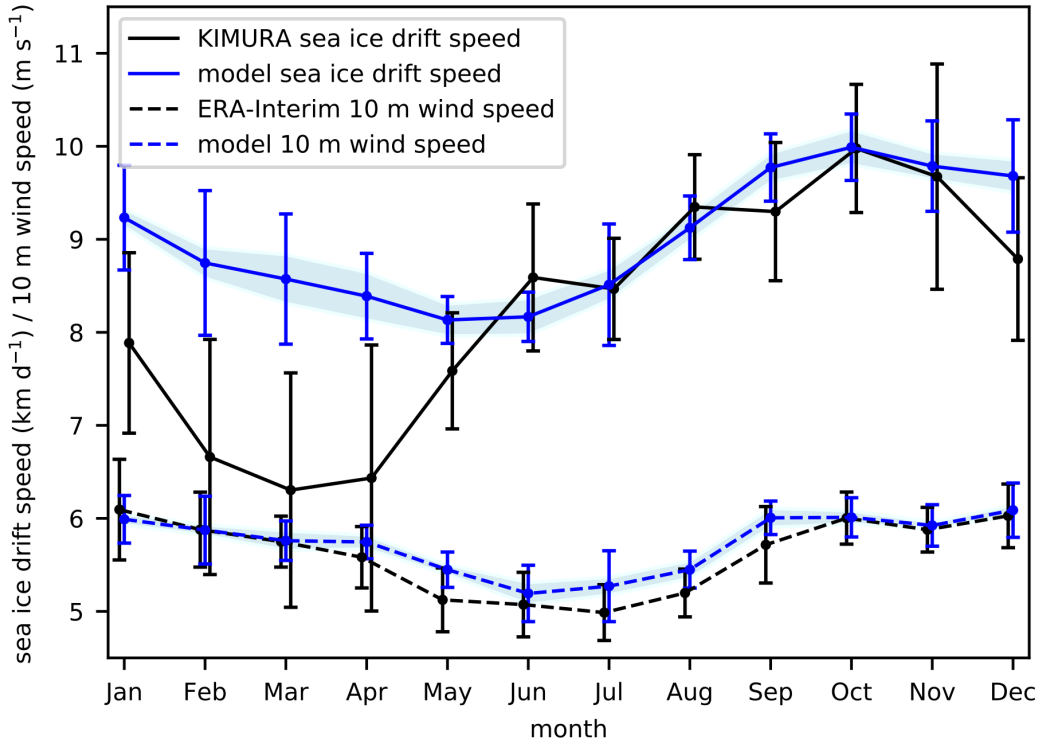


**Figure 2**: Mean annual cycle of sea-ice drift speed [km d$^{-1}$] (solid lines) and 10-m wind speed [m s$^{-1}$] (dashed lines), based on the model (ensemble mean; blue lines) and observation/reanalysis (KIMURA ice drift, ERA-I wind; black lines), 2003-2014 over the study domain (indicated in Figure 1). The across-ensemble scatter (standard deviation) of the simulations is included as shaded area. The interannual variation is shown by error bars.

https://doi.org/10.5194/tc-2019-183
Preprint. Discussion started: 26 August 2019




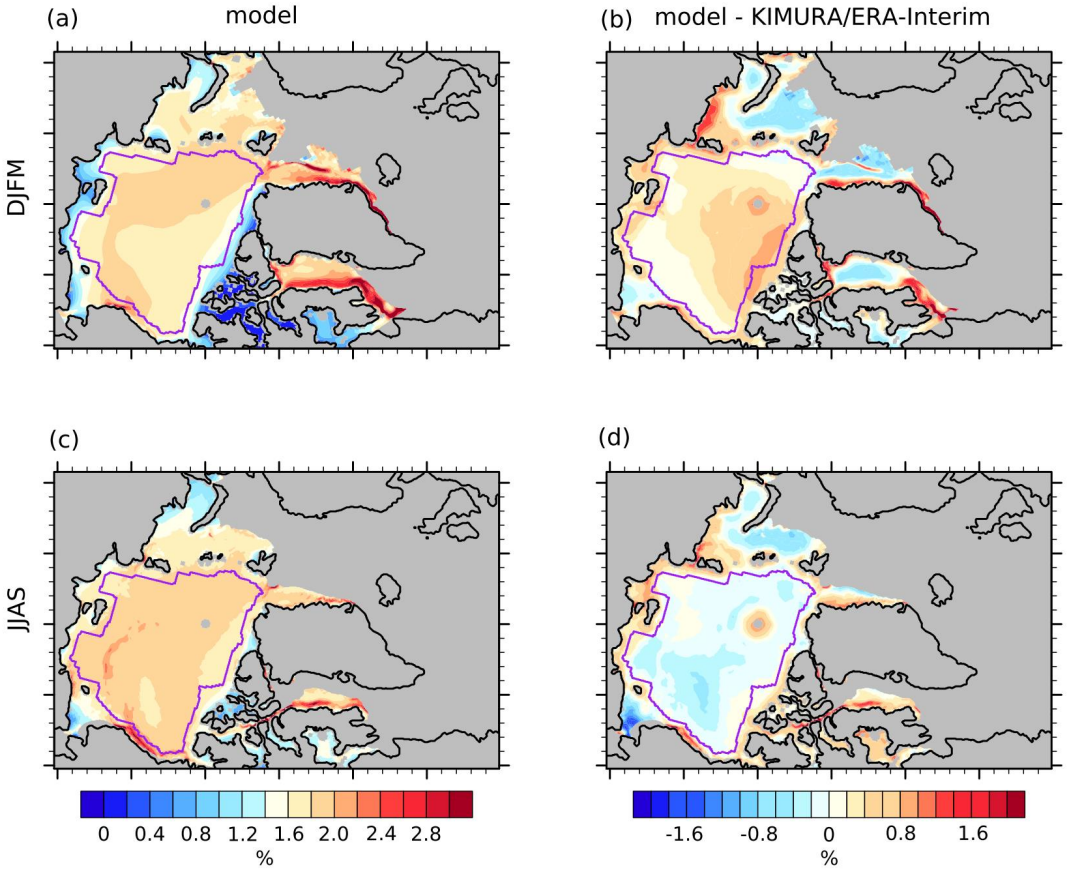


**Figure 3**: Mean spatial pattern of wind factor [%] in the model (ensemble mean) for 2003-2014 (a) winter (DJFM) and (c) summer (JJAS). (b) and (d) are the model differences to the observation/reanalysis ("Model - KIMURA/ERA-I") during winter and summer respectively. The purple line indicates the study domain used for the basin-wide analysis.

https://doi.org/10.5194/tc-2019-183
Preprint. Discussion started: 26 August 2019


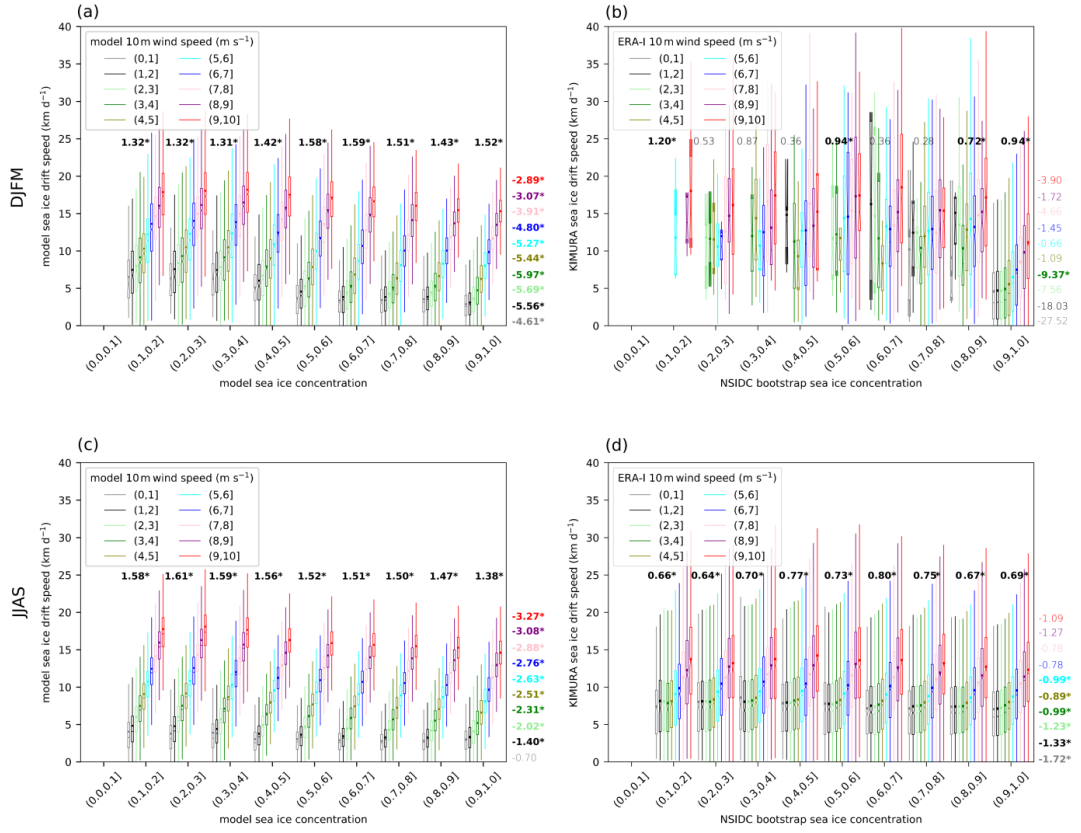


**Figure 4**: Box-whisker plots of the relationship between sea-ice drift speed and sea-ice concentration for different near-surface wind speed classes (different colors) in the model during 2003-2014 (a) winter (DJFM) and (c) summer. (b) and (d) are the relationship based on observation/reanalysis data during 2003-2014 winter and summer respectively. For the model, all 10 ensemble members are included. The plot is based on daily data and on all grid points within the study domain indicated in Figure 1. The horizontal bar represents the median, the notch represents the 95% confidence interval of the median, the dot represents the mean, the top and bottom of the box represent the 75th and 25th percentiles, the upper/lower whiskers represent the maximum/minimum value within 1.5 times interquartile range (IQR) to 75/25 percentiles. The numbers above the boxplots represent the slopes of near-surface wind and sea-ice drift speed fit lines (unit: km $d^{-1}$ per 1 m $s^{-1}$ wind speed change; font colors as for the wind speed classes). The numbers right of the boxplots represent the slopes of sea-ice concentration and sea-ice drift speed fit lines (unit: km $d^{-1}$ per 10% sea-ice concentration change). A bold and asterisked number indicates that the slope of the fit line is significant at the 95 % level.

https://doi.org/10.5194/tc-2019-183
Preprint. Discussion started: 26 August 2019


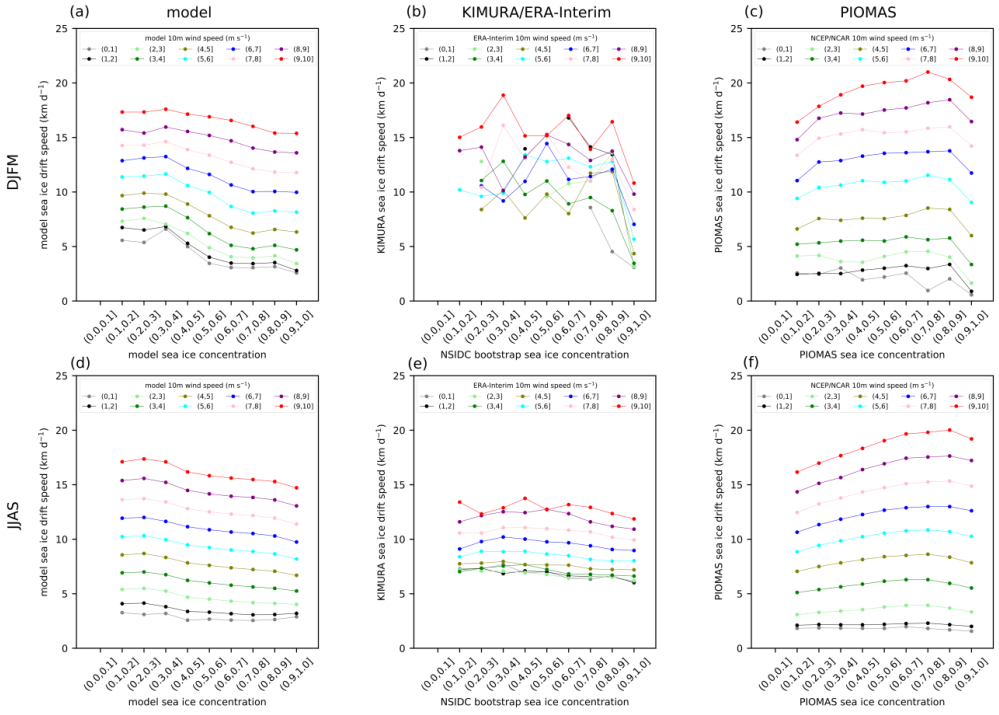


**Figure 5**: Relationship between sea-ice drift speed and sea-ice concentration for different near-surface wind speed classes (different colors) in the model during 2003-2014 (a) winter (DJFM) and (d) summer (JJAS). (b) and (e) are based on observation/reanalysis data. (c) and (f) are based on PIOMAS data. The points in the plot are the median value of all the daily data and on all grid points for certain wind speed and sea-ice concentration, within the study domain indicated in Figure 1.

https://doi.org/10.5194/tc-2019-183
Preprint. Discussion started: 26 August 2019


The Cryosphere Discussions
Open Access
EGU

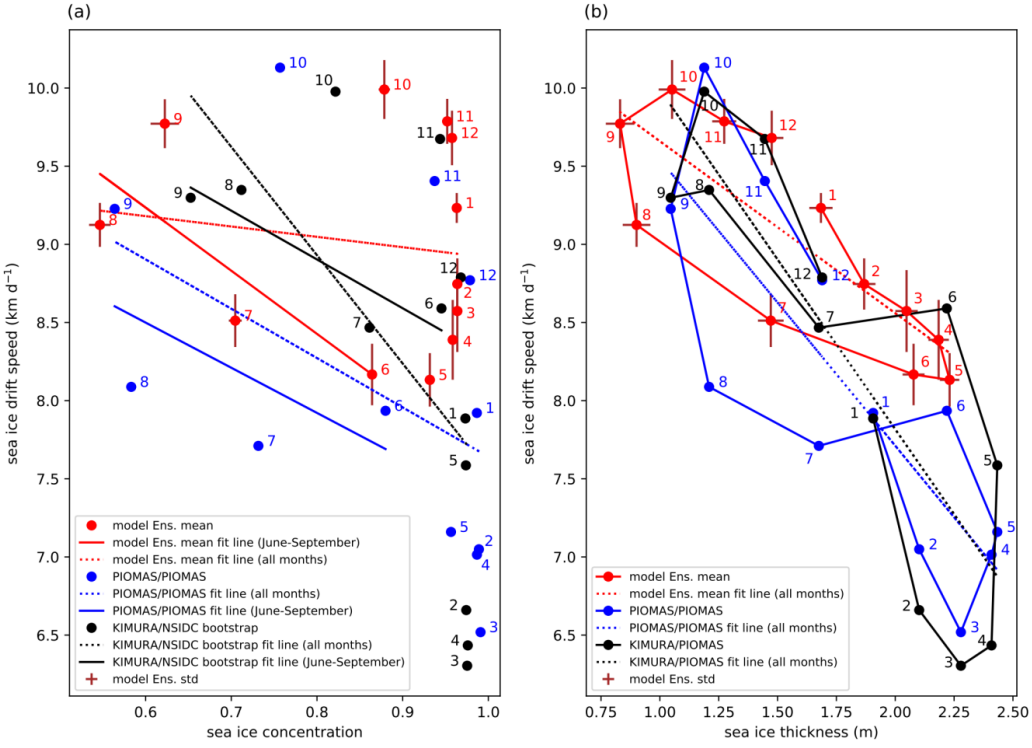


610

**Figure 6**: Scatter plots of monthly mean sea-ice drift speed against (a) sea-ice concentration and (b) sea-ice thickness, averaged over 2003-2014 and the study domain (indicated in Figure 1). Numbers denote the months. Results are shown for model ensemble simulations (red), KIMURA for ice drift speed plus NSIDC bootstrap for ice concentration (black), and PIOMAS data (blue).

https://doi.org/10.5194/tc-2019-183
Preprint. Discussion started: 26 August 2019


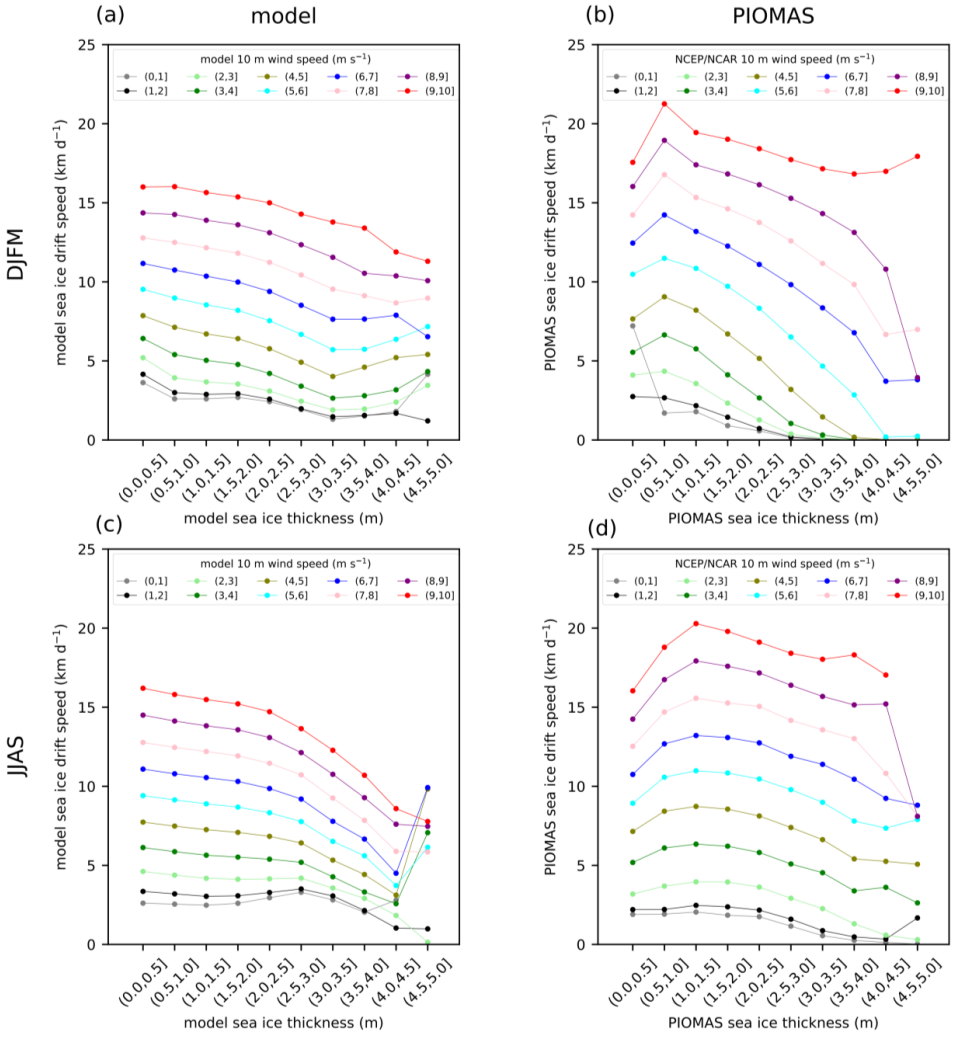


615

**Figure 7**: Relationship between sea-ice drift speed and sea-ice thickness for different near-surface wind speed classes (different colors) in the model during 2003-2014 (a) winter (DJFM) and (d) summer (JJAS). (b) and (d) are based on PIOMAS data. The points in the plot are the median value of all the daily data and on all grid points within the study domain based on Figure S5.

https://doi.org/10.5194/tc-2019-183
Preprint. Discussion started: 26 August 2019




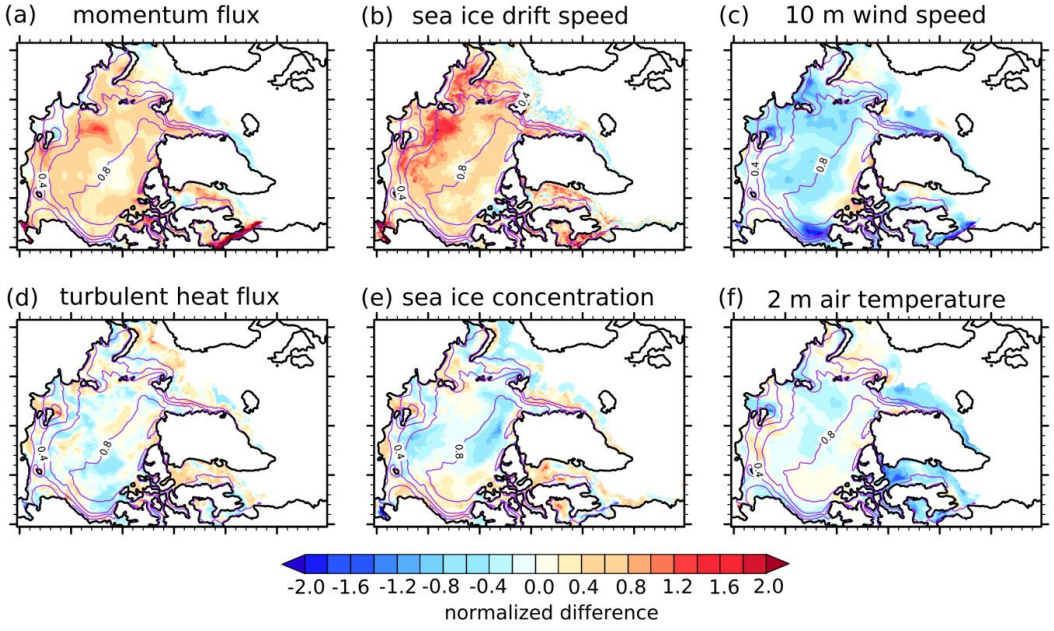


620

**Figure 8**: Normalized ensemble mean differences (SENS minus CTRL) of (a) momentum flux, (b) sea-ice drift speed, (c) 10-m wind speed, (d) turbulent heat flux, (e) sea-ice concentration, (f) 2 m air temperature during 2007 summer (JJAS). The ensemble mean difference is normalized by the cross-ensemble standard deviation of the differences. The purple contours represent the ensemble mean sea-ice concentration in the CTRL experiment.

https://doi.org/10.5194/tc-2019-183
Preprint. Discussion started: 26 August 2019


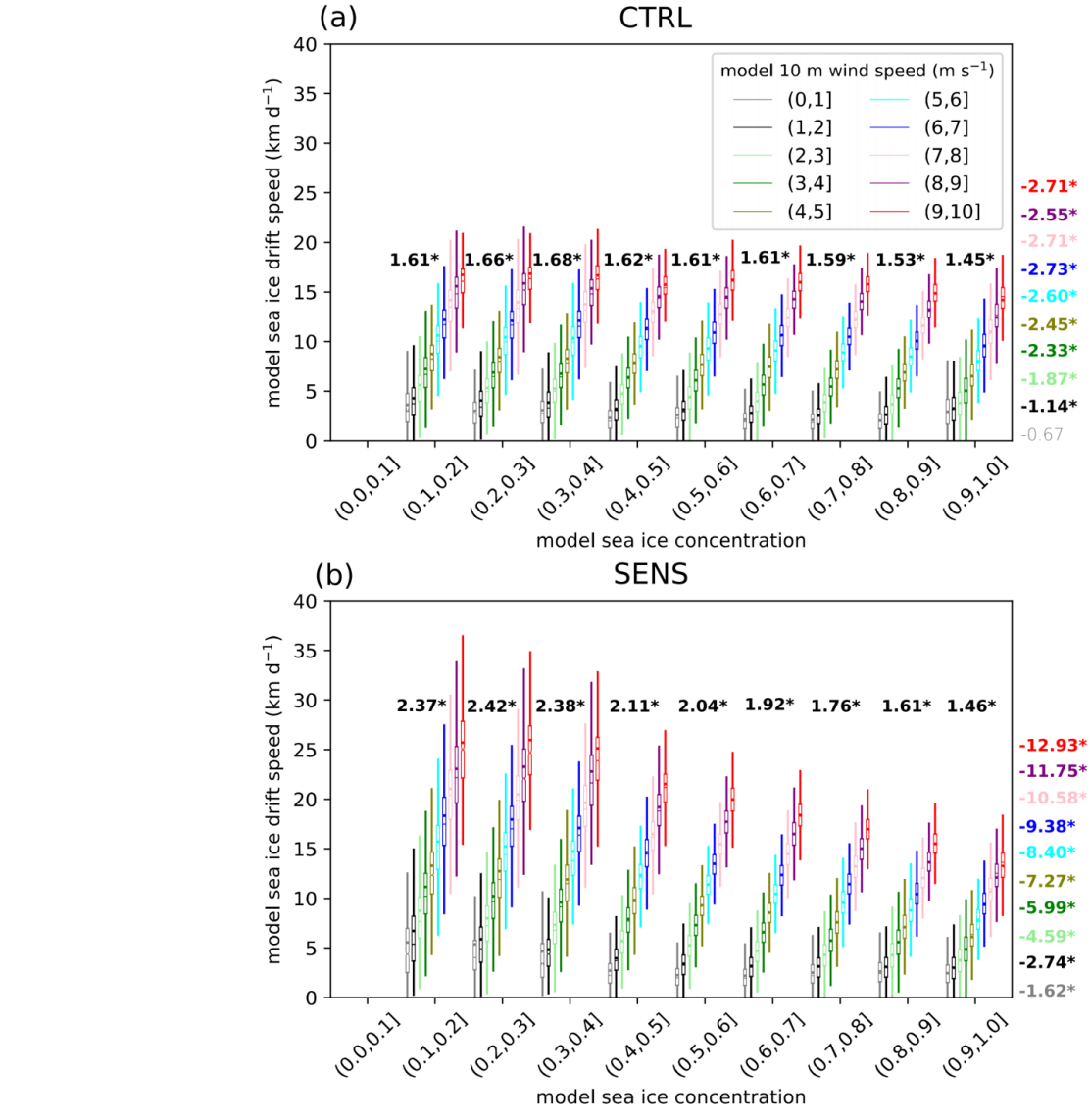


**Figure 9**: Box-whisker plots of the relationship between sea-ice drift speed and sea-ice concentration for different near-surface wind speed classes (different colors) during 2007 summer (JJAS) in (a) CTRL and (b) SENS experiment. The plot is based on daily data and on all grid points within the study domain indicated in Figure 1. The horizontal bar represents the median, the notch represents the 95% confidence interval of the median, the dot represents the mean, the top and bottom of the box represent the 75th and 25th percentiles, the upper/lower whiskers represent the maximum/minimum value within 1.5 times interquartile range (IQR) to 75/25 percentiles. The numbers above the boxplots represent the slopes of near-surface wind and sea-ice drift speed fit lines (unit: km d$^{-1}$ per 1 m s$^{-1}$ wind speed change; font colors as for the wind speed classes). The numbers right of the boxplots represent the slopes of sea-ice concentration and sea-ice drift speed fit lines (unit: km d$^{-1}$ per 10% sea-ice concentration change). A bold and asterisked number indicates that the slope of the fit line is significant at the 95 % level.

https://doi.org/10.5194/tc-2019-183
Preprint. Discussion started: 26 August 2019




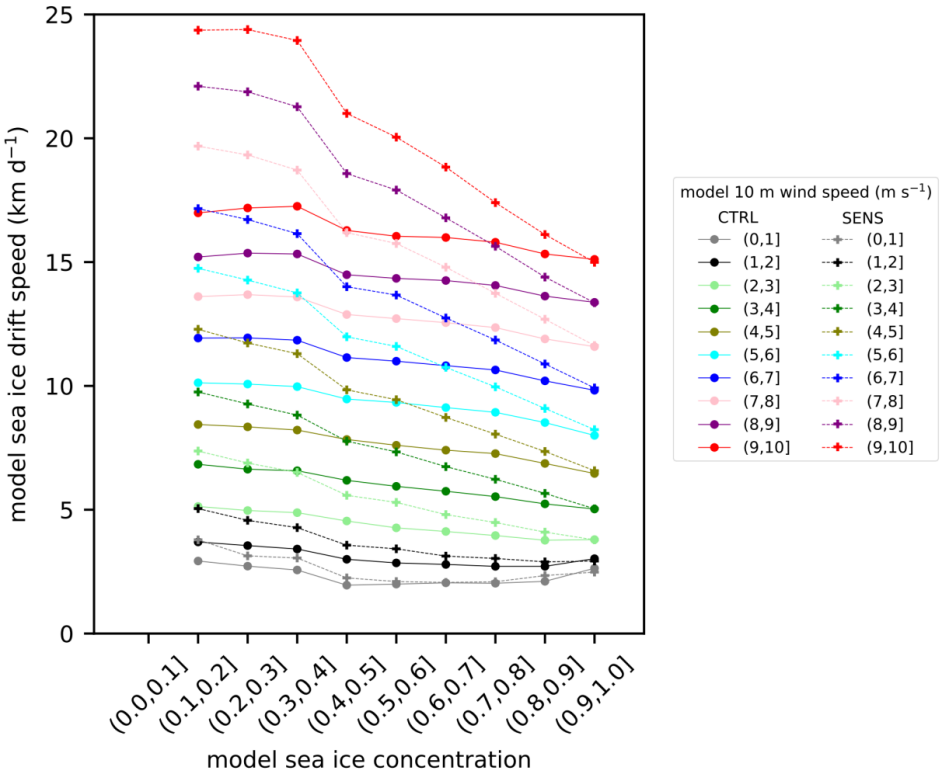


**Figure 10:** Relationship between sea-ice drift speed and sea-ice concentration for different near-surface wind speed classes (different colors) during 2007 summer (JJAS) for CTRL (circle marker and solid line) and SENS (cross marker and dash line) experiment. The points in the plot is the median value of all the daily data and on all grid points within the study domain indicated in Figure 1 under certain wind speed and sea-ice concentration classes.